Ab initio calculation of the miscibility diagram for mixtures of hydrogen and water

Armin Bergermann, Martin French ⬤, and Ronald Redmer ⬤
Institut für Physik, Universität Rostock, D-18051 Rostock, Germany

We calculate the miscibility gap in mixtures of hydrogen and water under high-temperature and high-pressure conditions as relevant for planetary interiors with density functional theory combined with classical molecular dynamics. In contrast to earlier calculations, we find a miscibility gap at temperatures below 1500–2000 K at pressures of up to 300 kbar, which extends the experimentally known immiscibility region by one order of magnitude in pressure. In contrast to extrapolated experimental demixing lines reaching to high temperatures, our results indicate a termination of the demixing region close to 2000 K. This finding profoundly impacts the understanding of the interiors of ice-giant planets such as Neptune and Uranus by supporting a partially demixed interior, including a density discontinuity near 2000 K, which corresponds to planetary radii of 0.85–0.95 in Uranus and Neptune. Additionally, our findings are relevant for thermal evolution models of Earth that aim to explain the formation of superreducing mineral associations.

I. INTRODUCTION

Neptune and Uranus are usually assumed to be ice-giant planets, consisting mostly of mixtures of the ice-forming compounds water, ammonia, and methane [1–3]. Since space probe missions to these ice giants are utterly challenging and expensive [4,5], knowledge gain on the interior structures of Uranus and Neptune relies mainly on the development and improvement of models [3,6–8]. For instance, an adiabatic temperature profile with three distinct layers, a rocky core, an inner layer rich in water, ammonia, and methane, and an outer layer rich in H_2 and He was commonly assumed [1,6,9–14]. These relatively simple models have density discontinuities at the boundaries between the three layers, which were assumed to keep the number of degrees of freedom as low as possible. Nevertheless, alternative classes of models of Uranus and Neptune with a continuous density profile were also developed [15,16]. In general, adiabatic interior models cannot explain the thermal evolution and very different brightnesses of Uranus and Neptune [17,18], which hints towards much more complex interior structures being present in ice giants [19]. Any credible planetary model needs to be based on a reliable thermophysical material database for the equation of state and phase diagram of the constituent mixture of compounds. For instance, an immiscibility region of H_2 and H_2O in the interiors of Uranus and Neptune could indeed lead to layer formation accompanied by density discontinuities in the planets' interiors [1,6,10,11,20]. The demixing process would also inhibit heat transport by convection, invalidating the assumption of an adiabatic interior and necessitating nonadiabatic models. Several nonadiabatic models have already been proposed by, e.g., Nettelmann *et al.* [14] and Scheibe *et al.* [18], to explain thermal evolution and brightness, assuming that primordial heat is trapped inside the planet. Recently, Bailey and Stevenson [21] discussed the impact of an H_2-H_2O miscibility gap in Uranus and Neptune. They found that the partial immiscibility of hydrogen and water could offer a solution to questions regarding the structure, magnetic field, and thermal evolution of ice-giant planets.

So far, three experimental studies have investigated the immiscibility region in water and hydrogen: In 1981, Seward and Franck [22] performed experiments with pressure vessels and determined immiscibility up to pressures of 2.3 kbar and temperatures of 650 K. In 2013, Bali *et al.* [23] used Raman spectroscopy to determine whether hydrogen and water entrapments in silicates can demix. They explored the respective miscibility gap at temperatures between 1000 and 1500 K and pressures between 17 and 25 kbar. In 2023, Vlasov *et al.* [24] used a similar experimental technique and confirmed the experimental findings of Bali *et al.* [23].

Interestingly, the experiments by Bali *et al.* [23] and Vlasov *et al.* [24] resulted in a demixing line with an upward curvature, which would lead to a very large demixing region extending to temperatures of several 1000 K when extrapolated. However, fundamental thermodynamics of mixtures requires termination of any demixing region at some temperature as the entropy rises [25,26], which occurs probably at pressure conditions that cannot be reached within current experimental setups.

Up to now, two contradicting theoretical predictions regarding the immiscibility of H_2 and H_2O are available. In 2015, Soubiran and Militzer [27] predicted H_2 and H_2O mixtures to be completely miscible by calculating the free enthalpy of mixing. They combined density functional theory (DFT) with molecular dynamics (MD). The coupling-constant integration technique [28] (CCI) was used to determine the nonideal entropy of the H_2-H_2O mixtures.

Recently, Bergermann *et al.* [29] conducted Gibbs ensemble Monte Carlo (GEMC) simulations using analytical two-body interaction potentials to describe the interaction between the molecular species H_2 and H_2O. A demixing diagram was predicted at pressures below 150 kbar and temperatures of $1000\,K < T < 2000\,K$. Notably, the isentropes

of Neptune and Uranus and the Archean geotherms are within the demixing region predicted by Bergermann *et al.* [29].

In this paper, we reinvestigate the miscibility diagram of hydrogen and water using *ab initio* simulations based on density functional theory combined with molecular dynamics (DFT-MD). We calculate the free enthalpy of mixing at temperatures between 1000 and 2000 K and pressures between 40 and 300 kbar. The CCI method [28,30] was used to determine the nonideal entropy, similarly to Soubiran and Militzer [27]. We consider nuclear quantum corrections (NQCs) of the ionic motion using a postprocessing method designed by Berens *et al.* [31,32]. This procedure influences the results significantly, as the immiscibility region is widened, which is shown below. A detailed explanation of the numerical techniques used is given in the Supplemental Material [33]. In contrast to Soubiran and Militzer [27], our simulations provide strong evidence for a miscibility gap in mixtures of hydrogen and water under high-pressure and high-temperature conditions, in agreement with the experimental findings and the GEMC simulations.

II. METHODS

We calculate the miscibility of hydrogen and water by evaluating differences in the free enthalpy in dependence on the water concentration. The free enthalpy per molecule g of the mixture is given by

$$\frac{G}{N_{\mathrm{H_2}} + N_{\mathrm{H_2O}}} = g = u + pv - Ts, \quad (1)$$

where u is the internal energy per molecule, p is the pressure, v is the volume per molecule, T is the temperature, and s is the entropy per molecule, G is the total free enthalpy, and $N_{\mathrm{H_2}}$ and $N_{\mathrm{H_2O}}$ are the numbers of hydrogen and water molecules, respectively. The free enthalpy of mixing is defined as

$$\Delta g(p, T, x) = g(p, T, x) - xg(p, T, 1)$$
$$- (1 - x)g(p, T, 0), \quad (2)$$

where $g(p, T, x)$ is the free enthalpy of the mixture, $g(p, T, 1)$ the free enthalpy of pure water, and $g(p, T, 0)$ that of pure hydrogen. Herein, x defines the molecular water fraction as follows,

$$x = \frac{N_{\mathrm{H_2O}}}{N_{\mathrm{H_2}} + N_{\mathrm{H_2O}}}. \quad (3)$$

A concave region indicates that the mixture is unstable and demixes into two phases with different concentrations [27,34–38]. By fitting $\Delta g(T, p, x)$ using a Redlich-Kister ansatz [39] and applying a double-tangent construction to $\Delta g(T, p, x)$, the concentrations of the water-poor and water-rich regions of the demixed fluid can be determined [26,34,35,37].

We performed DFT-MD simulations using the Vienne *ab initio* simulation package (VASP) [40–44]. We used the Perdew, Burke, and Ernzerhof (PBE) exchange-correlation functional [45] and the Nosé-Hoover thermostat [46,47] to maintain the temperature in the NVT ensemble. The thermodynamic variables p, T, u, and v are a direct output of our DFT-MD simulations. In contrast, the entropy is not directly available from the simulations. Unfortunately, the simplest
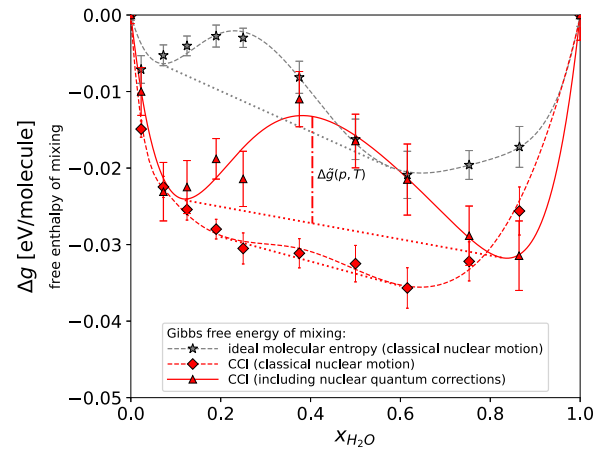

FIG. 1. Free enthalpy of mixing Δg as function of the water fraction $x_{\mathrm{H_2O}}$ for 1000 K and 120 kbar. Results from classical nuclear motion using the ideal molecular entropy: gray stars. Results calculated with the CCI method are shown in red, specifically: using the classical nuclear motion as red diamonds, by including the NQC as red triangles. The double-tangent constructions are depicted as dotted lines. The dashed-dotted line quantifies the size of the free enthalpy salient (concave section) $\Delta \tilde{g}(p, T)$ [see Eq. (4)].

approximation, the ideal molecular entropy of mixing, is insufficient for this purpose [34]. Therefore, we use the CCI method to calculate the nonideal entropy. Furthermore, we augment our simulation data for classical particles with the correction procedure of Berens *et al.* [31] to take into account NQC to the ionic motion. A more detailed description is given in the Supplemental Material [33].

Figure 1 illustrates the influences of the nonideal entropy and of NQC at 120 kbar and 1000 K. Using the ideal molecular mixing entropy and no NQC, we found an immiscibility region for water concentrations of $0.1 < x < 0.6$. The dotted lines represent the constructed double tangents. Using the nonideal entropy instead generally decreases the free enthalpy of mixing and reduces the concave section, which enhances the tendency of hydrogen and water to mix. By including the NQC, however, the concave region is widened, and we find a sizable immiscibility region for water concentrations of $0.1 < x < 0.85$.

The trends explained above are similar to what was found in earlier work on hydrogen-helium mixtures, where Schöttler *et al.* [34,35] observed that NQCs contributed significantly to Δg and enhanced the immiscibility in the molecular regime. These results underline the importance of the NQC when calculating the miscibility gap in molecular mixtures. Microscopically, NQCs originate mainly from changes in the vibrational properties of the molecules with x in our method.

Our results contradict the findings of Soubiran and Militzer [27,48], who found no demixing at all, partially because they did not take into account NQC. Furthermore, they applied less stringent convergence criteria in their DFT-MD simulation parameters. We were able to use up to two times more particles, two times more concentrations, up to two times more λ-integration points, and up to ten times longer simulation runs to diminish fluctuations and to obtain more precise results. A detailed overview is given in the Supplemental Material [33].
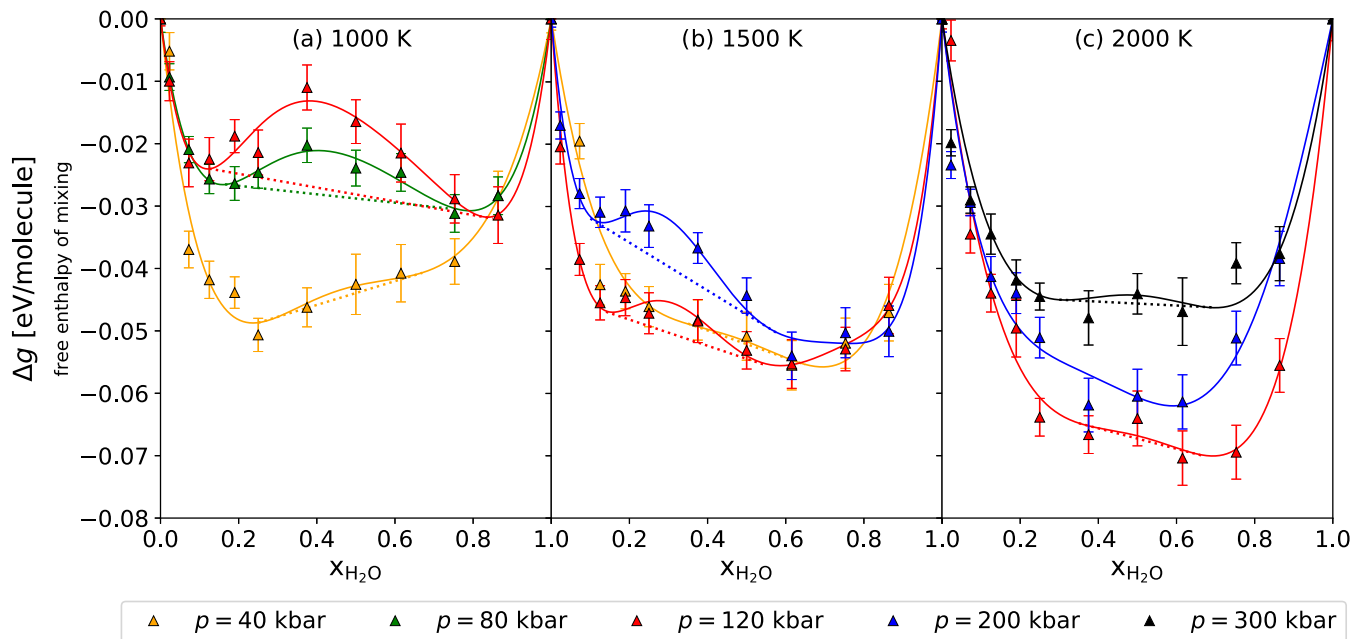
FIG. 2. Free enthalpy of mixing Δg for different p-T conditions. (a)–(c) show Δg for $T = 1000$, 1500, and 2000 K, respectively. Our raw data are shown by colored triangles. The solid lines are Redlich-Kister fits [39]. The dashed lines represent the double-tangent constructions.

III. STATISTICAL AND NUMERICAL ERRORS

To ensure the fidelity of our results, we calculated error bars to address statistical and numerical uncertainties. The uncertainty of the CCI, denoted as u_{CCI}, was determined by propagating the uncertainties arising from the DFT-MD simulations for different λ values. It is important to note that this procedure tends to overestimate the uncertainty. Our analysis reveals uncertainties ranging between 0.001 and 0.004 eV/molecule for the CCI. Comparatively, the uncertainty in pressure is an order of magnitude smaller than u_{CCI}, rendering the former negligible. Additionally, we account for the uncertainty associated with the NQC u_{NQC}. We find that including u_{NQC} enhances the total uncertainty to approximately $u_{NQC} = 0.000\,15$.

Finally, because of our much longer simulation times, more λ integration points, twice as many water concentrations, and higher particle numbers, we were able to reduce the statistical uncertainties significantly compared to the work of Soubiran and Militzer [27].

IV. RESULTS FOR THE DEMIXING REGION

Our main results for Δg at nine different p-T conditions are shown in Fig. 2. The free enthalpy of mixing is smallest for the lowest temperature (1000 K, left) and the lowest pressure (40 kbar). Increasing the temperature leads to a general decrease in Δg, a typical sign of temperature-enhanced solubility of water and hydrogen in each other. The same behavior occurs as the pressure is decreased, which reduces the influence of molecular interactions and effectively increases the ideality of the mixture.

At four conditions (1000 K: 80 and 120 kbar; 1500 K: 120 and 200 kbar), the free enthalpies of mixing show very pronounced concave behaviors, which implies that water and hydrogen are demixed there.

At the remaining five conditions (1000 K: 40 kbar; 1500 K: 40 kbar; 2000 K: 120, 200, and 300 kbar), we deem the numerical precision of the data points may not be sufficient to warrant the deduction of a significant concave region, although Redlich-Kister fit curves with slightly concave sections can be derived. Especially at he highest temperature of 2000 K (right panel in Fig. 2), the relatively straight sections in the Redlich-Kister fits indicate that this temperature is close to the highest one at which demixing can be expected in the pressure range between 120 and 300 kbar. The same holds for the condition of 1500 K and 40 kbar.

We did not calculate the free enthalpy for $p > 300$ kbar because these conditions intersect with the melting line of water [49–57]. The treatment of melting is not feasible within the present simulation approach. Likewise, it was not feasible to calculate the free enthalpy of mixing at pressures below 40 kbar because the DFT-MD simulations would have been computationally too expensive to obtain sufficiently precise results.

In general, the behavior of Δg in p-T space indicates that increasing the temperature reduces the miscibility gap in hydrogen-water mixtures. According to our data, hydrogen and water tend to become completely miscible above 2000 K between 40 and 300 kbar.

To quantify the demixing region, i.e., to determine the demixing line $T_d(p)$, which separates the miscible region from potentially demixed states, we quantify the size of the concave sections in our nine free enthalpies by determining the differences between $\Delta g(p, T, x)$ and the respective double tangent $\Delta g_t(p, T, x)$ at each value $x_i(p, T)$ where both functions have the same slope:

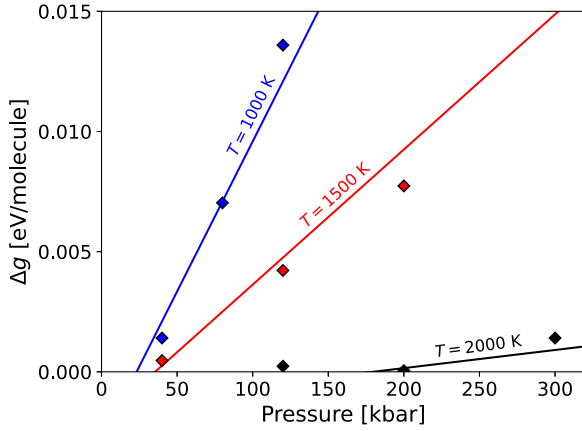$$\Delta \tilde{g}(p, T) = \Delta g(p, T, x_i) - \Delta g_t(p, T, x_i) \qquad (4)$$

FIG. 3. Results for $\Delta\tilde{g}(p,T)$ at 1000 K (blue), 1500 K (red), and 2000 K (black). The solid lines represent the corresponding fit from Eq. (5), which has a linear pressure dependence.

(see also Fig. 1 for an illustrative example). The quantity $\Delta\tilde{g}(p,T)$ shows a systematic behavior with p and T (see Fig. 3). The following functional form,

$$\Delta\tilde{g}(p,T) = a + bp + (c + ep)T^d, \qquad (5)$$

where a, b, c, d, e are coefficients given in Table I, allows for an accurate mathematical representation of $\Delta\tilde{g}(p,T)$ (see Fig. 3).

The zero of $\Delta\tilde{g}(p,T)$ naturally defines the lowest pressure $p(T)$ at which demixing occurs in the p-T plane. These values represent the demixing line $T_d(p)$ that is shown as a green line in Fig. 4.

Figure 4 also includes experimental results for demixing [22–24] and planetary isentropes [12,17]. Our demixing region is close to the experimental results of Bali *et al.* [23] and Vlasov *et al.* [24], deviating only by ≈ 2.5 kbar between 1000 and 1500 K and has a similarly steep slope as those from the experiments. However, at pressures above 50 kbar, our demixing line bends to the right and becomes nearly constant in temperature above 100 kbar. Interestingly, earlier results obtained from GEMC simulations which use classical pair potentials [29] are also in the vicinity of the present results.

Concluding this section, our results agree with the experimentally known immiscibility region and extend this region by one order of magnitude in pressure. For pressures above 100 kbar, we predict the highest temperature where demixing occurs to be almost constant. Thus, hydrogen and water become completely miscible above 2000 K.

V. IMPACT ON ICE GIANTS

The p-T diagram of water-hydrogen mixtures shown in Fig. 4 indicates that the thermal profiles through the ice giants Uranus and Neptune intersect with the demixing area
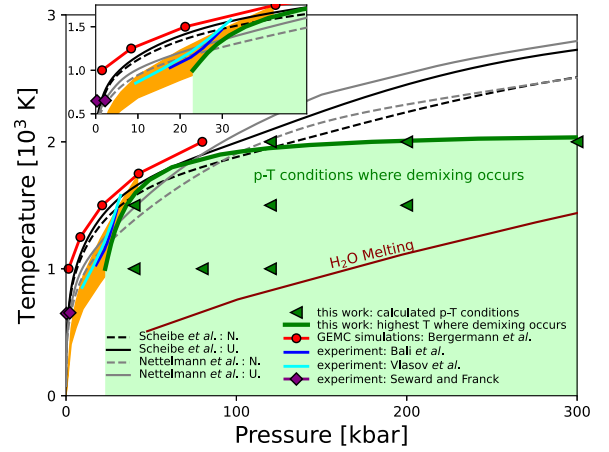

FIG. 4. T-p diagram with all conditions for which we calculated Δg (green triangles). The green demixing line $T_d(p)$ shows the lowest pressure and highest temperatures where demixing occurs according to the condition $\Delta\tilde{g}(p,T) = 0$ [see Eq. (5)]. For comparison we show GEMC results of Bergermann *et al.* [29] (red circles), experiments by Bali *et al.* [23] (blue line), experiments by Seward and Franck [22] (purple diamonds), and experiments by Vlasov *et al.* [24] (cyan line). The melting line of water is shown in dark red [58]. Predicted T-p profiles along Uranus' and Neptune's radius are shown by solid and dashed lines, respectively: Scheibe *et al.* [17] (black) and Nettelmann *et al.* [12] (model N1: gray). We also added Earth's Archean geotherms as given by Mareschal and Jaupart [59] (orange shaded area). The inset shows the low-pressure region in more detail.

calculated in this work. Therefore, we expect hydrogen and water to be immiscible in certain regions of the ice giant planets.

According to the planetary model N1 for Neptune by Nettelmann *et al.* [12], immiscibility of hydrogen and water can occur at radii between $r_N = 0.86\,R_N$ and $r_N = 0.93\,R_N$, where $R_N = 24\,622$ km denotes the radius of Neptune. They predict a jump in density at $r_{N\rho} = 0.86\,R_N$ which is within our demixing region. For the planetary model of Uranus [12] immiscibility of hydrogen and water can occur at radii between $r_U = 0.83\,R_U$ and $r_U = 0.87\,R_U$, where $R_U = 25\,362$ km denotes the radius of Uranus. The jump in density is predicted at $r_{U\rho} = 0.77\,R_U$ and, therefore, very close to our demixing region. Note, however, that a certain minimum concentration of water is required to cause demixing of hydrogen and water, which depends nonlinearly on p and T. Figure 2 indicates that demixing occurs when the water fraction reaches approximately $\approx 15\%$ at temperatures of 1000 and 1500 K.

The miscibility gap of hydrogen and water supports the assumption of density discontinuities inside ice-giant planets. Therefore, more complex planetary models than the adiabatic interior assumption are required to explain heat transport from the warm-to-hot center towards the cool surface [15]. For

TABLE I. Coefficients for the fit formula, Eq. (5).

a (eV)	b (eV/kbar)	c (eV/K)	d	e [eV/(K × kbar)]
−3.1119382	0.2364756	3.0937059	0.0007158	−0.235185

example, Nettelmann *et al.* [12] proposed a model with a boundary at about 100 kbar and 2000 K. At these T-p conditions, hydrogen and water might be immiscible, resulting in a stably stratified layer with a density jump. Therefore, heat transport by convection would be inhibited, leading to primordial heat trapped inside the planet, while the relatively thin outer layer is cooling rapidly (see Scheibe *et al.* [18] for a detailed study).

Furthermore, our demixing curve intersects with Earth's Archean geotherms as well. Therefore, our results support the assumption of the formation of superreducing mineral associations and rapid upper mantle oxidation [23,24,60] and subsequently influence the evolution of Earth and Earth-like exoplanets.

In conclusion, our work provides predictions for the miscibility gap of hydrogen and water mixtures at pressures and temperatures, and especially quantifies the *p*-*T* region in which the demixing terminates in the interior. These findings will help to better understand giant ice plan-ets such as Neptune and Uranus but also Neptune-like exoplanets, which are a very common class of exoplanets. Our findings provide valuable insights that will aid in developing new planetary models capable of addressing long-standing scientific questions regarding the structure and evolution of Uranus and Neptune and influence future space missions [4].

[1] W. B. Hubbard and J. J. MacFarlane, J. Geophys. Res. **85**, 225 (1980).

[2] W. B. Hubbard, Science **214**, 145 (1981).

[3] J. J. Fortney and N. Nettelmann, Space Sci. Rev. **152**, 423 (2010).

[4] C. Arridge, N. Achilleos, J. Agarwal, C. Agnor, R. Ambrosi, N. André, S. Badman, K. Baines, D. Banfield, M. Barthélémy, M. Bisi, J. Blum, T. Bocanegra-Bahamon, B. Bonfond, C. Bracken, P. Brandt, C. Briand, C. Briois, S. Brooks, J. Castillo-Rogez *et al.*, Planet. Space Sci. **104**, 122 (2014).

[5] A. Masters, N. Achilleos, C. Agnor, S. Campagnola, S. Charnoz, B. Christophe, A. Coates, L. Fletcher, G. Jones, L. Lamy, F. Marzari, N. Nettelmann, J. Ruiz, R. Ambrosi, N. Andre, A. Bhardwaj, J. Fortney, C. Hansen, R. Helled, G. Moragas-Klostermeyer *et al.*, Planet. Space Sci. **104**, 108 (2014).

[6] R. Helled, N. Nettelmann, and T. Guillot, Space Sci. Rev. **216**, 38 (2020).

[7] R. Helled and T. Guillot, in *Handbook of Exoplanets*, edited by H. Deeg and J. Belmonte (Springer, Berlin, 2018), pp. 167–185.

[8] T. Guillot, Exp. Astron. **54**, 1027 (2022).

[9] W. B. Hubbard, W. J. Nellis, A. C. Mitchell, N. C. Holmes, S. S. Limaye, and P. C. McCandless, Science **253**, 648 (1991).

[10] M. S. Marley, P. Gómez, and M. Podolak, J. Geophys. Res. **100**, 23349 (1995).

[11] M. Podolak, A. Weizman, and M. Marley, Planet. Space Sci. **43**, 1517 (1995).

[12] N. Nettelmann, R. Helled, J. Fortney, and R. Redmer, Planet. Space Sci. **77**, 143 (2013).

[13] M. Bethkenhagen, E. R. Meyer, S. Hamel, N. Nettelmann, M. French, L. Scheibe, C. Ticknor, L. A. Collins, J. D. Kress, J. J. Fortney, and R. Redmer, Astrophys. J. **848**, 67 (2017).

[14] N. Nettelmann, K. Wang, J. Fortney, S. Hamel, S. Yellamilli, M. Bethkenhagen, and R. Redmer, Icarus **275**, 107 (2016).

[15] M. Podolak, R. Helled, and G. Schubert, Mon. Not. R. Astron. Soc. **487**, 2653 (2019).

[16] R. Helled and J. J. Fortney, Philos. Trans. R. Soc. A **378**, 20190474 (2020).

[17] L. Scheibe, N. Nettelmann, and R. Redmer, Astron. Astrophys. **632**, A70 (2019).

[18] L. Scheibe, N. Nettelmann, and R. Redmer, Astron. Astrophys. **650**, A200 (2021).

[19] M. French and N. Nettelmann, Astrophys. J. **881**, 81 (2019).

[20] M. Podolak, J. Podolak, and M. Marley, Planet. Space Sci. **48**, 143 (2000).

[21] E. Bailey and D. J. Stevenson, Planet. Sci. J. **2**, 64 (2021).

[22] T. M. Seward and E. U. Franck, Bunsen-Ges. Phys. Chem., Ber. **85**, 2 (1981).

[23] E. Bali, A. Audétat, and H. Keppler, Nature (London) **495**, 220 (2013).

[24] K. Vlasov, A. Audétat, and H. Keppler, Contrib. Mineral. Petrol. **178**, 36 (2023).

[25] S. M. Walas, *Phase Equilibria in Chemical Engineering* (Butterworth-Heinemann, Oxford, UK, 1985).

[26] M. de Oliveira, *Equilibrium Thermodynamics*, Graduate Texts in Physics (Springer, Berlin, 2014).

[27] F. Soubiran and B. Militzer, Astrophys. J. **806**, 228 (2015).

[28] J. G. Kirkwood, J. Chem. Phys. **3**, 300 (1935).

[29] A. Bergermann, M. French, and R. Redmer, Phys. Chem. Chem. Phys. **23**, 12637 (2021).

[30] O. Sugino and R. Car, Phys. Rev. Lett. **74**, 1823 (1995).

[31] P. H. Berens, D. H. J. Mackay, G. M. White, and K. R. Wilson, J. Chem. Phys. **79**, 2375 (1983).

[32] M. Bethkenhagen, M. French, and R. Redmer, J. Chem. Phys. **138**, 234504 (2013).

[33] See Supplemental Material at http://link.aps.org/supplemental/10.1103/PhysRevB.109.174107 for details on the calculation of entropies, which includes Refs. [27,28,30–32,34–38,40–47,53].

[34] M. Schöttler and R. Redmer, Phys. Rev. Lett. **120**, 115703 (2018).

[35] M. Schöttler and R. Redmer, J. Plasma Phys. **85**, 945850201 (2019).

[36] M. A. Morales, S. Hamel, K. Caspersen, and E. Schwegler, Phys. Rev. B **87**, 174105 (2013).

[37] W. Lorenzen, B. Holst, and R. Redmer, Phys. Rev. Lett. **102**, 115701 (2009).

[38] M. A. Morales, C. Pierleoni, E. Schwegler, and D. M. Ceperley, Proc. Natl. Acad. Sci. USA **107**, 12799 (2010).

[39] O. Redlich and A. T. Kister, Ind. Eng. Chem. **40**, 345 (1948).

[40] G. Kresse and J. Hafner, Phys. Rev. B **47**, 558 (1993).

[41] G. Kresse and J. Hafner, Phys. Rev. B **49**, 14251 (1994).

[42] G. Kresse and J. Furthmüller, Comput. Mater. Sci. **6**, 15 (1996).

[43] G. Kresse and J. Furthmüller, Phys. Rev. B **54**, 11169 (1996).

[44] J. Hafner, J. Comput. Chem. **29**, 2044 (2008).

[45] J. P. Perdew, K. Burke, and M. Ernzerhof, Phys. Rev. Lett. **77**, 3865 (1996).

[46] S. Nosé, Prog. Theor. Phys. Suppl. **103**, 1 (1991).

[47] W. G. Hoover, Phys. Rev. A **31**, 1695 (1985).

[48] F. Soubiran and B. Militzer, High Energy Density Phys. **17**, 157 (2015).

[49] T. Kimura and M. Murakami, J. Chem. Phys. **158**, 134504 (2023).

[50] J.-F. Lin, E. Gregoryanz, V. V. Struzhkin, M. Somayazulu, H.-k. Mao, and R. J. Hemley, Geophys. Res. Lett. **32**, L11306 (2005).

[51] E. Schwegler, M. Sharma, F. Gygi, and G. Galli, Natl. Acad. Sci. Lett. USA **39**, 14779 (2008).

[52] R. Redmer, T. R. Mattsson, N. Nettelmann, and M. French, Icarus **211**, 798 (2011).

[53] M. French, New J. Phys. **21**, 023007 (2019).

[54] J.-A. Queyroux, J.-A. Hernandez, G. Weck, S. Ninet, T. Plisson, S. Klotz, G. Garbarino, N. Guignot, M. Mezouar, M. Hanfland, J.-P. Itié, and F. Datchi, Phys. Rev. Lett. **125**, 195501 (2020).

[55] B. Schwager, L. Chudinovskikh, A. Gavriliuk, and R. Boehler, J. Phys.: Condens. Matter **16**, S1177 (2004).

[56] B. Schwager and R. Boehler, High Press. Res. **28**, 431 (2008).

[57] T. Kimura, Y. Kuwayama, and T. Yagi, J. Chem. Phys. **140**, 074501 (2014).

[58] L. Zhang, H. Wang, R. Car, and W. E, Phys. Rev. Lett. **126**, 236001 (2021).

[59] J.-C. Mareschal and C. Jaupart, in *Archean Geodynamics and Environments*, edited by K. Benn, J.-C. Mareschal, and K.C. Condie, Geophysical Monograph Series Vol. 164 (American Geophysical Union, Washington, DC, 2006), p. 61.

[60] Z. D. Sharp, F. M. McCubbin, and C. K. Shearer, Earth Planet. Sci. Lett. **380**, 88 (2013).